Journal of Materials Chemistry C

Accepted Manuscript

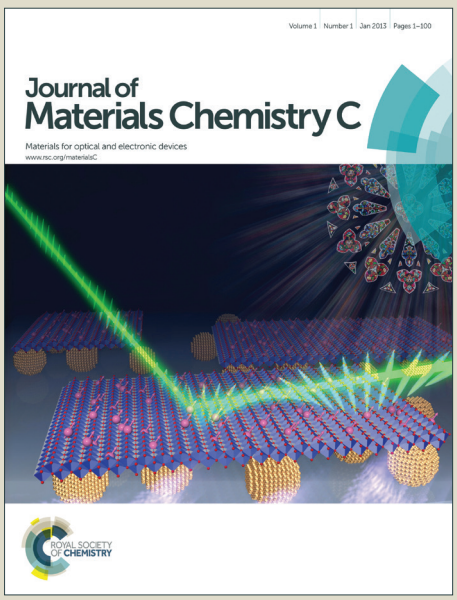

ROYAL SOCIETY OF CHEMISTRY

www.rsc.org/materialsC

Journal Name

RSCPublishing

ARTICLE

Creating SERS Hot Spots on Ultralong Single-Crystal β-$AgVO_3$ Microribbons

Cite this: DOI: 10.1039/x0xx00000x

Seung-Ho Jang,‡ Jun Hee Yoon,‡ Young-Duk Huh, and Sangwoon Yoon*

Received 00th January 2012,
Accepted 00th January 2012

DOI: 10.1039/x0xx00000x

www.rsc.org/

β-$AgVO_3$ ribbons are a novel one-dimensional structure with excellent structural, electric, and catalytic properties. Here we report the synthesis of ultralong β-$AgVO_3$ microribbons and their applications as a surface-enhanced Raman scattering (SERS) substrate. A hydrothermal method allows us to prepare millimeter-long β-$AgVO_3$ ribbons with a cross section of ~2.5 μm × ~1 μm with a high yield. The length of the β-$AgVO_3$ microribbons is controlled by the amount of pyridine added to $AgNO_3$ and NH_4VO_3. The perfectly smooth and single crystalline β-$AgVO_3$ surfaces drastically change into rough and rippled surfaces upon reaction with 4-aminothiophenol. Electron microscopy studies reveal that Ag nanoparticles with a diameter of ~ 7 nm are formed on the surface, rendering the ultralong β-$AgVO_3$ microribbons highly SERS-active. Possible mechanisms of the transformation and applications of the resulting SERS-active substrates in microfluidics are discussed.

Introduction

One-dimensional beta-silver vanadate (β-$AgVO_3$) ribbons hold a great potential for a variety of applications due to their unique properties. The layered structures and superior ionic properties make them an ideal cathodic electrode for lithium batteries.[1-3] Semiconducting characteristics of β-$AgVO_3$ ribbons also allow them to be used as catalysts, antibacterial agents, gas sensors, and nanoelectronic devices.[4-8]

Many efforts have been made to produce long β-$AgVO_3$ ribbons. Wet chemical methods as well as hydrothermal methods have been extensively used.[3,9-13] However, the lengths of the resulting β-$AgVO_3$ ribbons have been limited to a few hundred microns.

Here we report a facile synthesis of millimeter-long β-$AgVO_3$ microribbons. We also present morphological transformation of the resulting ultralong microribbons to surface-enhanced Raman scattering (SERS)-active materials.

SERS is a highly sensitive spectroscopic method that provides both chemical and structural information on molecules near nanostructures.[14,15] SERS arises from intense localized electromagnetic fields around the noble metal nanoparticles, produced by the resonant interaction of light with surface plasmons of the metal nanoparticles.[16] Due to the drastically increased Raman scattering intensity, typically six to ten orders of magnitude, and rich information that it can provide, SERS has been widely used in bio- and chemosensing, single molecule spectroscopy, and cancer cell detection.[17-20]

Toward more diverse applications of SERS, developing robust, reproducible, and easily makeable SERS-active substrates is required. In particular, one-dimensional SERS-active materials are highly demanded for microfluidic SERS sensors. For the SERS detection in microfluidics, microchannel surfaces are usually modified *in situ* to render them SERS-active.[21,22] External preparation of SERS-active microstrips can be a good alternative approach for better quality-controlled fabrication of sensors. To this end, synthesis of one-dimensional ultralong β-$AgVO_3$ microribbons and their transformation into SERS-active materials is an important first step.

Experimental

Preparation of ultralong β-$AgVO_3$ microribbons

$AgNO_3$ (99%, Aldrich), pyridine (99%, Aldrich), NH_4VO_3 (99%, Aldrich), and 4-aminothiophenol (4-ATP, 97%, Aldrich) were used as received without further purification. Ultralong β-$AgVO_3$ ribbons were prepared by a hydrothermal method. Pyridine (3.26 mL) was added to 34.0 mL of 12 mM $AgNO_3$ solution. The solution was then added to 40.0 mL of 18 mM NH_4VO_3 solution. The resulting mixture was transferred to a 100-mL autoclave and heated at 180 °C for 3 h. The β-$AgVO_3$ product was filtered, washed with water and ethanol, and dried for 12 h at room temperature. The amount of pyridine was changed from 3.26 to 0.326 mL, corresponding to the molar ratio of pyridine to $AgNO_3$ 100 to 10.

4-ATP treatment

The β-$AgVO_3$ product (2 mg) was dispersed in 2 mL of water by sonication, and then mixed with 1 mL 4-ATP solution in ethanol. The concentration of the 4-ATP solution varied from 0.5 mM to 10 mM. After 4 h, the 4-ATP-treated samples were filtered, washed with ethanol several times, and then dried.

Measurements

The structure and morphology of β-$AgVO_3$ product was characterized by powder X-ray diffraction (XRD, PANalytical,

X'pert-pro MPD), scanning electron microscopy (SEM, Hitachi, S-4300), and high-resolution transmission electron microscopy (HRTEM, JEOL, JEM-3010). Raman spectra were acquired using a Raman microscope (Kaiser, RamanRxn Microprobe). Samples were placed on a quartz plate and transferred to an optical microscope (Leica, DMLP). A diode laser (785 nm, 12 mW) was focused on the sample through an objective with 50× magnification. Raman scattering was collected by the same objective and transmitted to a holographic spectrometer (f/1.8) by optical fibers. Total exposure time for each spectrum was 1 s unless otherwise noted. For Raman mapping, a region of 35 μm × 33 μm was scanned and Raman spectra were acquired at 20 × 20 spots. The Raman intensity at 1076 cm^{-1} (C–S stretching mode of 4-ATP) was mapped to find the SERS intensity distribution on the β-$AgVO_3$ microribbons

Results and discussion

We synthesized β-$AgVO_3$ microribbons using a hydrothermal method. A mixture of $AgNO_3$, pyridine, and NH_4VO_3 was prepared in a molar ratio of 1 : 100 : 1.75 and was heated in an autoclave at 180 °C for 3 h. The yielded yellow powder was characterized using SEM and XRD. The SEM images show that the synthesized product consists of ultralong wires as long as 2 mm (Figure 1a). The tilt view of SEM reveals that the wires have a flat, squashed circular cross section rather than a round circle, resembling a section cut face of a sword. The width and the height of the cross sections are ~2.5 and ~1 μm, respectively (Figure 1a inset). We note that millimeter-long microribbon structures are very rare. To the best of our knowledge, the longest β-$AgVO_3$ ribbon reported so far was approximately 300 μm.[13,23]

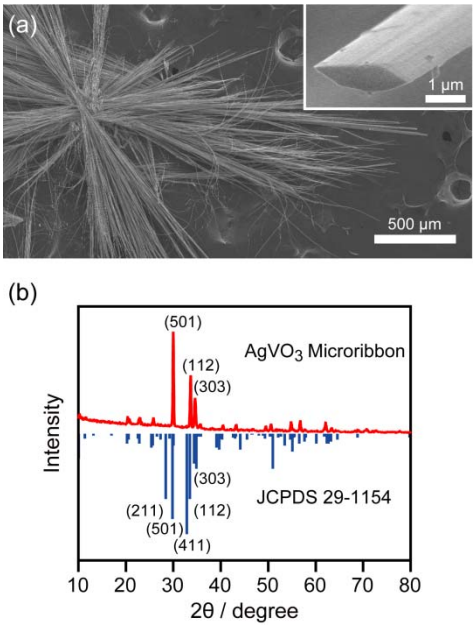

Figure 1. (a) A representative SEM image and (b) XRD spectrum of the prepared ultralong β-$AgVO_3$ microribbons. The inset in (a) is the cross sectional view of the structures obtained from the tilt SEM. The XRD pattern of the monoclinic β-$AgVO_3$ crystals from the database is included upside down for comparison (blue line).

An XRD analysis indicates that the prepared ribbon structures are single crystalline β-$AgVO_3$ (Figure 1b). The XRD pattern of the product matches with the reported data of monoclinic β-$AgVO_3$ crystal structures (JCPDS 29-1154, a = 1.787 nm, b = 0.3580 nm, c = 0.8036 nm, β = 101.33°). No other peaks are observed, indicating that the product is impurity-free β-$AgVO_3$. Furthermore, the strongest (501) peak and almost invisible (211) and (411) peaks in the XRD spectrum of the product, compared to the spectrum from the database, suggest that the β-$AgVO_3$ microribbons grow along the (501) lattice plane.

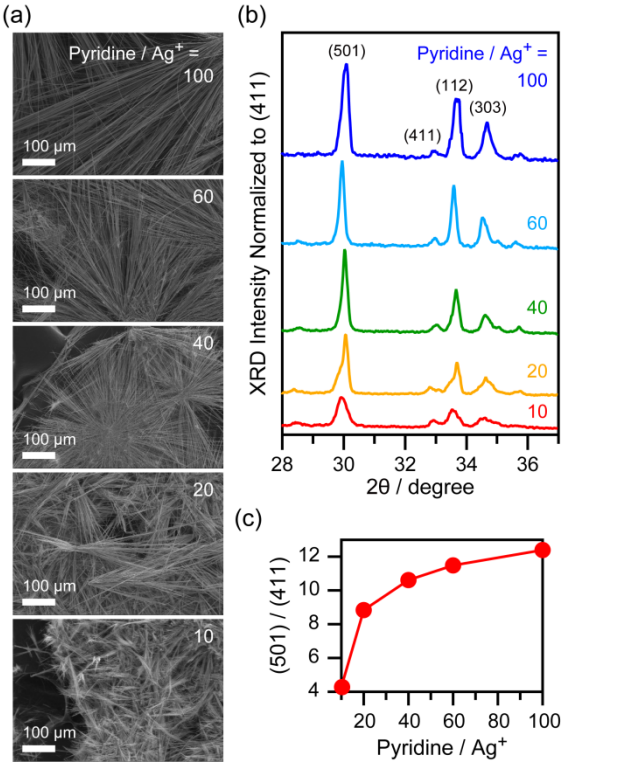

Figure 2. (a) Representative SEM images and (b) XRD patterns of β-$AgVO_3$ microribbons as the molar ratio of pyridine to $AgNO_3$ in the synthesis increases from 10 to 100. (c) Relative diffraction peak intensity of (501) to (411) in the XRD spectra as a function of the molar ratio of pyridine to $AgNO_3$.

We found that the length of the β-$AgVO_3$ microribbons depends on the amount of pyridine. As the molar ratio of pyridine to $AgNO_3$ increases from 10 to 100, the length of the resulting β-$AgVO_3$ microribbons increases (Figure 2). The XRD data also indicate the growth of the β-$AgVO_3$ microribbons with the increasing amount of pyridine. The relative peak intensity of (501) to (411) increases as more pyridine is used in the synthesis (Figure 2b, 2c). The role of pyridine in the synthesis of β-$AgVO_3$ microribbons has been discussed in their pioneering work by Yu and co-workers.[13] Pyridine coordinates with silver ions and thereby controls the reaction rate for the formation of $AgVO_3$. It is not clear at this stage why the increase in the amount of pyridine induces directional growth of the β-$AgVO_3$ ribbons in our synthesis scheme. One possibility is that slow reaction of silver ions with VO_3^- due to the presence of abundant pyridine thermodynamically controls the reaction, leading to the preferential formation of $AgVO_3$ on the lattice plane with the highest surface energy.

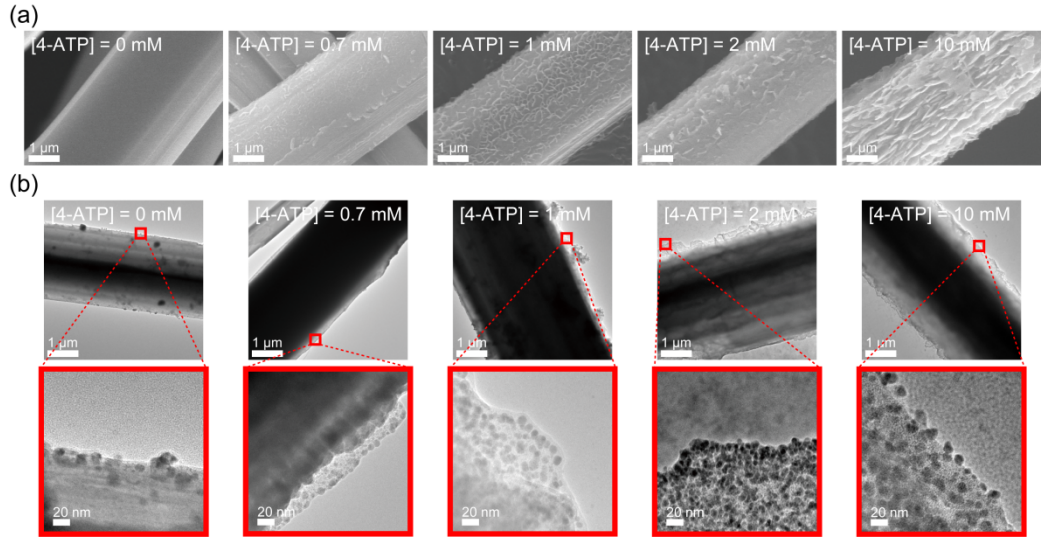

Figure 3. Structural evolution of β-$AgVO_3$ microribbons as they react with 4-ATP in 0, 0.7, 1.0, 2.0 and 10.0 mM. Images in (a) and (b) are SEM and TEM images after the reaction, respectively. Magnified TEM images, enclosed in the red squares, are also presented in (b).

The morphology of the β-$AgVO_3$ microribbons undergoes drastic changes upon addition of 4-ATP. The β-$AgVO_3$ product was dispersed in water and mixed with 4-ATP solution in concentrations ranging from 0.5 mM to 10 mM. The color of the 4-ATP-treated β-$AgVO_3$ microribbons visibly changes from yellow to green and finally to black as the concentration of the added 4-ATP increases. The SEM image in Figure 3a shows that the surface of the initially prepared β-$AgVO_3$ microribbons is perfectly clean and smooth ([4-ATP] = 0 mM). However, as they react with more concentrated 4-ATP, the surface becomes more and more rough and rippled. Such structural changes were further investigated with TEM. The TEM images in Figure 3b reveal that the initially solid structure of β-$AgVO_3$ microribbons turns transparent on the periphery upon reacting with 4-ATP as if the surface partially dissolved. As more concentrated 4-ATP is used, small dots are formed on the surface. When the concentration of 4-ATP reaches 10 mM, the small dots grow to be 6.5 ± 2.2 nm in diameter and cover the whole surface of the β-$AgVO_3$ microribbons. Electron diffraction measurements on those small dots reveal that they are silver nanoparticles (AgNPs). The electron diffraction pattern in Figure 4 clearly displays the (111) and (200) lattice planes with lattice spacings of 2.3 and 2.0 Å, characteristic of ccp crystalline structures of Ag.[24]

Presence of abundant AgNPs on the ultralong β-$AgVO_3$ ribbons strongly suggests possible plasmonic effects from the surface.[16] We investigated the SERS activity of the β-$AgVO_3$ microribbons as they were treated with increasing concentrations of 4-ATP. Figure 5 shows that the pristine β-$AgVO_3$ microribbons ([4-ATP] = 0 mM) exhibit a typical Raman spectrum of $AgVO_3$. The Raman peaks at 732, 808, and 886 cm^{-1} correspond to the Ag–O–Ag stretching, VO_3 group-stretching, and V–O–Ag or V–O–V stretching vibrational modes, respectively, in excellent agreement with previous

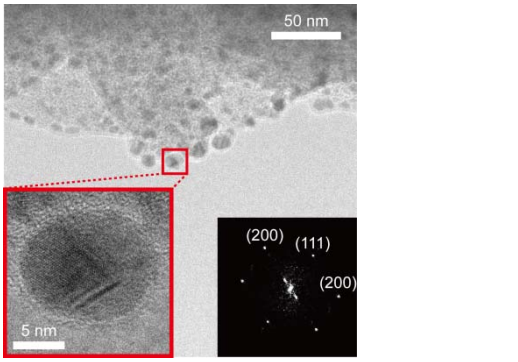

Figure 4. A TEM image of AgNPs formed on the β-$AgVO_3$ microribbons by the reaction with 10 mM 4-ATP. The inset presents the electron diffraction fast Fourier transform image of the selected particle, enclosed in the red square.

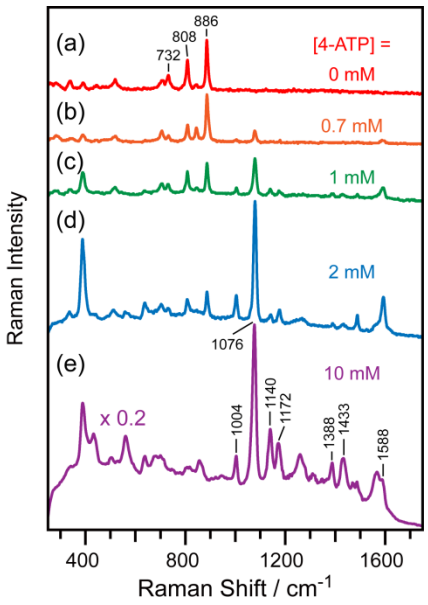

Figure 5. Raman spectral evolution of β-$AgVO_3$ microribbons as they react with 4-ATP in (a) 0, (b) 0.7, (c) 1.0, (d) 2.0 and (e) 10.0 mM. Note that the Raman spectrum in (e) is scaled down by a factor of 0.2.

studies.[13,25] As the β-$AgVO_3$ microribbons are treated with more concentrated 4-ATP, those Raman peaks decrease in intensity and eventually vanish. Instead, new Raman peaks rise at 1004, 1076, 1140, 1172, 1388, 1433, and 1588 cm^{-1}. The Raman spectrum obtained from β-$AgVO_3$ microribbons treated with 10 mM of 4-ATP perfectly matches with the SERS spectrum of 4-ATP previously reported from Ag or Au nanoparticle aggregates.[26,27] Abundant nanogaps in AgNP aggregates significantly enhance the Raman intensity of the a_1-symmetry vibrational modes of 4-ATP at 1004, 1076, 1172, and 1588 cm^{-1} *via* electromagnetic enhancement.[27-29] Additionally, the peaks at 1140, 1388, and 1433 cm^{-1} are an important signature of SERS from charge transfer between 4-ATP and AgNPs or photocatalytic reaction of 4-ATP on AgNPs.[29,30] Therefore, the observation of SERS from the β-$AgVO_3$ microribbons unambiguously indicates the formation of AgNP aggregates on the microribbon surfaces and adsorption of 4-ATP molecules on those AgNPs. The SERS enhancement factor (EF) for the 4-ATP-treated β-$AgVO_3$ microribbons is conservatively estimated to be 1×10^7 (Supporting Information).

The evolution of Raman spectra is consistent with the structural transformation of the β-$AgVO_3$ microribbons, observed through SEM and TEM in Figure 3. The initially prepared β-$AgVO_3$ microribbons have single crystalline structures with smooth surfaces, giving rise to Raman spectrum of pure $AgVO_3$. Upon addition of 4-ATP, the surface becomes roughened and eventually small AgNPs are formed on the surface. In this structure, the 4-ATP molecules that adsorb on the AgNPs generate the strong SERS signal.

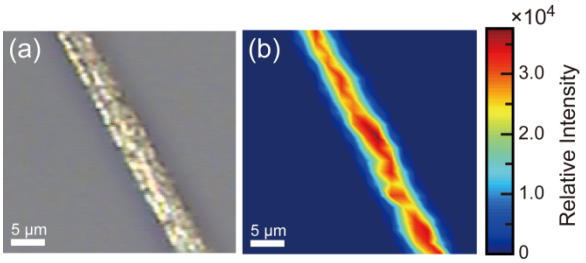

Figure 6. (a) Optical image and (b) SERS mapping of the 4-ATP-treated β-$AgVO_3$ microribbons.

SERS occurs all over the surfaces of the 4-ATP-treated β-$AgVO_3$ ribbon structures. The SERS mapping for the 1076 cm^{-1} peak (C–S stretching mode of 4-ATP) in Figure 6 shows that the intensity is relatively evenly distributed in a large region, indicating that AgNPs are formed throughout the β-$AgVO_3$ ribbon surfaces that have reacted with 4-ATP. This result also suggests that the ultralong β-$AgVO_3$ ribbons may serve well as an excellent SERS-generating one-dimensional microstructure.

The formation of AgNPs on the surface of β-$AgVO_3$ microribbons is specifically induced by the reaction with thiol (–SH). Figure 7 shows that β-$AgVO_3$ microribbons do not react with aniline or phenol. Consequently, Raman spectra of those β-$AgVO_3$ microribbons treated with aniline or phenol are the same as the Raman spectrum of pristine β-$AgVO_3$ microribbons. In contrast, significant structural changes occur when β-$AgVO_3$ microribbons react with 4-ATP and thiophenol, as shown in the SEM images in Figure 7a. SERS spectra also exhibit the spectral features of 4-ATP and thiophenol although the SERS intensity of the former is far larger than the latter. The

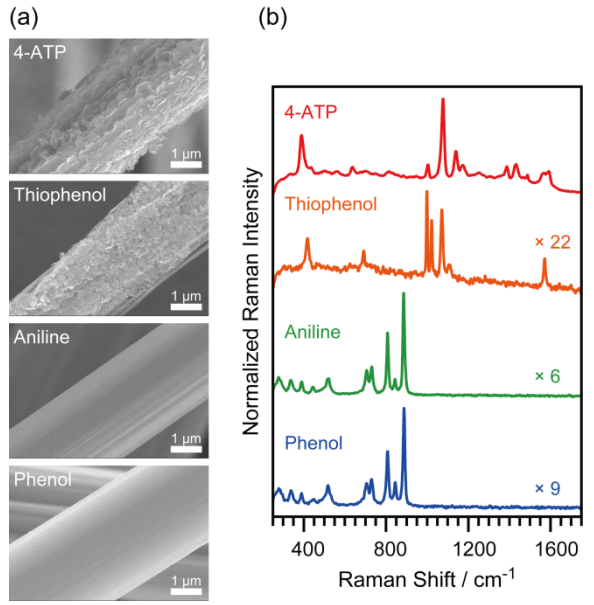

Figure 7. (a) SEM images and (b) Raman spectra of β-$AgVO_3$ microribbons treated with 4-ATP, thiophenol, aniline, and phenol.

difference in the SERS intensity between 4-ATP and thiophenol is presumably due to the size and density of AgNPs formed on the surface of the β-$AgVO_3$ microribbons. TEM images show that the AgNPs produced by the reaction with 4-ATP are ~ 7 nm in diameter and more densely distributed on the surface of the β-$AgVO_3$ microribbons, providing more hot spots for SERS. In contrast, the AgNPs formed by thiophenol seem to be yet premature; they are smaller (2.7 ± 1.4 nm) and more sparsely distributed, resulting in much weaker plasmonic effects (Supporting Information). We note that thiol is much more strongly activated in 4-ATP than in thiophenol due to the electron-donating character of amine, leading to a greater reactivity for the former than the latter.

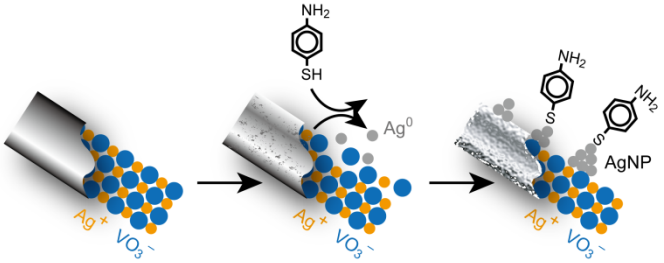

Figure 8. Proposed mechanism of the formation of AgNPs on the surface of ultralong β-$AgVO_3$ microribbons by the reaction with 4-ATP. The AgNPs on the surface give rise to strong SERS signal.

From these observations, we conclude that the SERS-activity of the ultralong β-$AgVO_3$ microribbons upon reaction with 4-ATP is closely related to the formation of AgNPs on the surface. In producing the AgNPs, the thiol group plays a pivotal role. Figure 8 illustrates our proposal on the transformation of the ultralong β-$AgVO_3$ microribbons into the SERS-active materials by 4-ATP. The initially prepared ultralong β-$AgVO_3$ microribbons have well-defined crystalline structures. Upon addition of 4-ATP, the 4-ATP molecules specifically reduce the

ionic silver that constitutes the β-$AgVO_3$ microribbon structures presumably due to the strong affinity of thiol toward silver. Reduction of ionic silvers results in dissolution of the surfaces of the β-$AgVO_3$ microribbons, as observed in the TEM images in Figure 3b. The silver atoms from the reduction produce AgNPs on the β-$AgVO_3$ microribbon surfaces. The formation of AgNPs on the surfaces makes the β-$AgVO_3$ microribbons look rough and rippled. The AgNPs yield the SERS signal of 4-ATP which chemisorbs on the AgNP surface via the formation of Ag–S bond.

The 4-ATP-treated ultralong β-$AgVO_3$ microribbons are an excellent one-dimensional SERS-active material. They have a comparable EF (~10^7) to other commonly used SERS substrates.[14] They are prepared in bulk quantities. The synthesis is simple and straightforward. Most of all, the unique one-dimensional structure (millimeter long and micrometer wide) of the prepared β-$AgVO_3$ microribbons is perfectly suited to microchannels, opening up new possibilities as a novel SERS substrate in microfluidic SERS sensors.

Conclusions

We produced ultralong single-crystal β-$AgVO_3$ microribbons using a hydrothermal method. The resulting product was as long as 2 mm and has a cross-section of ~2.5 μm × ~1 μm. The length was controllable by adjusting the amount of added pyridine in the synthesis. The XRD data revealed that the produced microribbons have monoclinic β-$AgVO_3$ crystal structures. The morphology of the β-$AgVO_3$ microribbons drastically changed upon reaction with 4-ATP. The surface turned rough and rippled from the perfectly smooth surface of the pristine β-$AgVO_3$ microribbons in the SEM images as 4-ATP was added. TEM images showed that small AgNPs were formed on the surface upon reaction with 4-ATP, that were responsible for rough appearance of the surface. Plasmonic effect of AgNPs also yielded strong SERS signal of 4-ATP from the β-$AgVO_3$ microribbons. We propose that the reduction of Ag ions in the β-$AgVO_3$ microribbons by the thiol of 4-ATP produces AgNPs. The millimeter-scale length and high SERS-activity of the β-$AgVO_3$ microribbons make them an ideal candidate for substrates of microfluidic SERS sensors.

Acknowledgements

This research was supported by Basic Science Research Program through the National Research Foundation of Korea funded by the Ministry of Education (NRF-2013R1A1A2008336 and NRF-2010-0007492).

Notes and references

Department of Chemistry, Dankook University, 152 Jukjeon-ro, Suji-gu, Yongin, Gyeonggi 448-701, Korea. E-mail: sangwoon@dankook.ac.kr

‡ These authors (SHJ and JHY) contributed equally.

Electronic Supplementary Information (ESI) available: Calculation of SERS enhancement factor and comparison of TEM images of β-$AgVO_3$ microribbons treated with 4-ATP and thiophenol. See DOI: 10.1039/b000000x/

1. M. S. Whittingham, *Chem. Rev.*, 2004, **104**, 4271-4301.
2. A.-M. Cao, J.-S. Hu, H.-P. Liang and L.-J. Wan, *Angew. Chem., Int. Ed.*, 2005, **44**, 4391-4395.
3. S.-J. Bao, Q.-L. Bao, C.-M. Li, T. P. Chen, C.-Q. Sun, Z.-L. Dong, Y. Gan and J. Zhang, *Small*, 2007, **3**, 1174-1177.
4. L. Mai, L. Xu, Q. Gao, C. Han, B. Hu and Y. Pi, *Nano Lett.*, 2010, **10**, 2604-2608.
5. M. Feng, L.-B. Luo, B. Nie and S.-H. Yu, *Adv. Funct. Mater.*, 2013, **23**, 5116-5122.
6. Q. Zhou, M. Shao, R. Que, L. Cheng, S. Zhuo, Y. Tong and S.-T. Lee, *Appl. Phys. Lett.*, 2011, **98**, 193110.
7. R. D. Holtz, F. A. G. Souza, M. Brocchi, D. Martins, N. Duran and O. L. Alves, *Nanotechnology*, 2010, **21**, 185102.
8. D. P. Das, R. K. Barik, J. Das, P. Mohapatra and K. M. Parida, *RSC Adv.*, 2012, **2**, 7377-7379.
9. S. Kittaka, Y. Yata, K. Matsuno and H. Nishido, *J. Mater. Sci.*, 2000, **35**, 2185-2192.
10. S. Sharma, M. Panthoefer, M. Jansen and A. Ramanan, *Mater. Chem. Phys.*, 2005, **91**, 257-260.
11. M.-W. Shao, L. Lu, H. Wang, S. Wang, M.-L. Zhang, D.-D.-D. Ma and S.-T. Lee, *Chem. Commun.*, 2008, 2310-2312.
12. S. Zhang, W. Li, C. Li and J. Chen, *J. Phys. Chem. B*, 2006, **110**, 24855-24863.
13. J.-M. Song, Y.-Z. Lin, H.-B. Yao, F.-J. Fan, X.-G. Li and S.-H. Yu, *ACS Nano*, 2009, **3**, 653-660.
14. C. L. Haynes, A. D. McFarland and R. P. Van Duyne, *Anal. Chem.*, 2005, **77**, 338A-346A.
15. J. P. Camden, J. A. Dieringer, J. Zhao and R. P. Van Duyne, *Acc. Chem. Res.*, 2008, **41**, 1653-1661.
16. M. Rycenga, C. M. Cobley, J. Zeng, W. Li, C. H. Moran, Q. Zhang, D. Qin and Y. Xia, *Chem. Rev.*, 2011, **111**, 3669-3712.
17. Y. C. Cao, R. Jin and C. A. Mirkin, *Science*, 2002, **297**, 1536-1540.
18. K. Kneipp, Y. Wang, H. Kneipp, L. T. Perelman, I. Itzkan, R. R. Dasari and M. S. Feld, *Phys. Rev. Lett.*, 1997, **78**, 1667-1670.
19. S. Nie and S. R. Emory, *Science*, 1997, **275**, 1102-1106.
20. X. Qian, X.-H. Peng, D. O. Ansari, Q. Yin-Goen, G. Z. Chen, D. M. Shin, L. Yang, A. N. Young, M. D. Wang and S. Nie, *Nat. Biotechnol.*, 2008, **26**, 83-90.
21. J. Parisi, L. Su and Y. Lei, *Lab Chip*, 2013, **13**, 1501-1508.
22. S. H. Yazdi and I. M. White, *Anal. Chem.*, 2012, **84**, 7992-7998.
23. J. Xu, C. Hu, Y. Xi, B. Wan, C. Zhang and Y. Zhang, *Solid State Sci.*, 2012, **14**, 535-539.
24. JCPDS 03-0921.
25. R. Lewandowska, K. Krasowski, R. Bacewicz and J. E. Garbarczyk, *Solid State Ionics*, 1999, **119**, 229-234.
26. K. Kim, J. K. Yoon, H. B. Lee, D. Shin and K. S. Shin, *Langmuir*, 2011, **27**, 4526-4531.
27. J. H. Yoon, J. S. Park and S. Yoon, *Langmuir*, 2009, **25**, 12475-12480.
28. K. Kim and J. K. Yoon, *J. Phys. Chem. B*, 2005, **109**, 20731-20736.
29. M. Osawa, N. Matsuda, K. Yoshii and I. Uchida, *J. Phys. Chem.*, 1994, **98**, 12702-12707.
30. Y.-F. Huang, H.-P. Zhu, G.-K. Liu, D.-Y. Wu, B. Ren and Z.-Q. Tian, *J. Am. Chem. Soc.*, 2010, **132**, 9244-9246.